



Low-Cycle Fatigue Behavior of Friction Stir-Welded Copper Joints

Ali Hosseinzadeh, Salar Salahi, Amin Radi, Seyed Vahid Sajadifar, and Guney Guven Yapici

Submitted: 8 February 2021 / Revised: 19 June 2021 / Accepted: 26 June 2021 / Published online: 20 July 2021

Investigation of the fatigue response of friction stir-welded (FSWed) joints is especially important in the design and manufacturing of components with exposure to cyclic loading. In this study, cyclic response of FSWed pure copper joints is investigated in the low-cycle fatigue regime. Microstructural characterizations revealed that FSW introduced a severely deformed microstructure in the nugget zone (NZ). Fatigue response was determined at a strain ratio of 0.1 by varying the total strain amplitude from 0.1 to 0.6%. Cyclic softening was observed for the low strain amplitude of 0.1%, whereas hardening was detected at higher strain amplitudes. The hysteresis loops demonstrated symmetry along with noticeable linear behavior after the reversals. Typical fractures occurred in the heat affected zone (HAZ) rather than the NZ or the base metal due to grain coarsening of the HAZ. Improved cyclic properties of the NZ along with stable behavior up to 1000 cycles at a total strain amplitude of 0.3% were attributed to its fine and homogeneous microstructure. Moreover, fracture surface analysis demonstrated a ductile behavior represented by dimples in the sample strained at 0.1% in contrast with a brittle fracture surface of the sample fatigued at 0.5% strain amplitude.

Keywords cyclic response, fracture, friction stir welding, mechanical behavior, low-cycle fatigue, pure copper

1. Introduction

As a tough, malleable, and ductile metal along with its good conductivity of heat and electricity, pure copper has been widely used for manufacturing various devices including integrated circuit boards, power transmission lines, and electric motors (Ref 1). On the other hand, recently, multiple applications in evaporators and heating coils push forward progressing the welding of pure copper (Ref 1, 2). Furthermore, diffusion of oxygen at high welding temperature throughout fusion welding significantly deteriorates the desired mechanical properties of copper joints (Ref 3, 4). Friction stir welding (FSW), as a solid-state joining approach, has been employed to eliminate the negative effects of conventional welding methods and enhance the strength of the joints (Ref 5-7). During FSW, the frictional heat generated from the bottom surface of the shoulder and pin increases the temperature of material below the melting temperature. Besides, plastic deformation by stirring the material around the pin leads to the formation of joints (Ref 8-10). From the microstructural perspective, decreasing the

volume fraction of porosities, elimination of cracks, and segregations has made FSW an appropriate selection for joining copper as well as light alloys such as magnesium and aluminum alloys (Ref 11-18).

The effect of FSW parameters such as traverse and rotational speed, plunge depth, and dimensions of the tool on the microstructure and mechanical behavior of copper joints under static loading has been previously reported in the literature (Ref 19, 20). Primary works discovered that the welding heat input for copper is higher than that of aluminum alloys (Ref 21), while further works were able to recognize the range of welding parameters for obtaining defect-free joints (Ref 22). For instance, Salahi et al. (Ref 23) studied the potential welding envelope for copper joints, distinguishing the impact of different welding parameters and reported elevated hardness values in the NZ due to the significant grain refinement. Although finer microstructure can be reached in the NZ by decreasing the heat input, the risk of defect formation increases (Ref 24, 25). Using response surface methodology, a comprehensive work was also performed to find the parameter range maximizing the tensile strength of pure copper joints (Ref 26).

Concerning the mechanical properties of joints under cyclic loading, few studies can be found on the fatigue behavior of FSWed aluminum alloys and its composites in the high-cycle fatigue (HCF) regime (Ref 27, 28). Hrishikesh et al. (Ref 28) reported that the HCF behavior of FSWed Al6061 at different stress ratios is mainly related to the welding parameters and microstructure of various FSW regions. While the HCF regime is mainly controlled by the level of stress, the low-cycle fatigue (LCF) is governed by the ductility which is highly sensitive to the process parameters affecting the microstructure (Ref 29). An attempt to investigate the LCF properties of AZ91D magnesium alloy was performed using the Basquin and Coffin–Manson equations (Ref 30). In the case of pure copper, LCF investigations have mainly emphasized the microstructure evolution of samples (Ref 31-33). Cyclic softening was

Ali Hosseinzadeh, Amin Radi, and Guney Guven Yapici, Mechanical Engineering Department, Ozyegin University, Istanbul, Turkey; and Mechanics and Manufacturing of Functional and Structural Materials Lab (MEMFIS), Ozyegin University, Istanbul, Turkey; Salar Salahi, Mechanical Engineering Department, Ozyegin University, Istanbul, Turkey; Seyed Vahid Sajadifar, Mechanical Engineering Department, Ozyegin University, Istanbul, Turkey; and Institut für Werkstofftechnik (Materials Engineering), Universität Kassel, 34125 Kassel, Germany. Contact e-mail: guven.yapici@ozyegin.edu.tr.

reported in severely deformed copper at high strain ranges due to a remarkable decrease in the dislocation density making it easier for dislocations to move during cyclic deformation (Ref 34). Systematic investigations in the past decade have revealed the dislocation evolution mechanism during LCF of pure copper. The process may involve the formation of loop patches, persistent slip bands (PSBs), cells, and finally misoriented cells (Ref 35-38).

Although few studies could be found on the LCF behavior of FSWed aluminum and magnesium joints (Ref 30, 39), there has been a lack of effort devoted to investigating the subject of FSWed copper joints. Importance of the cyclic deformation characteristics of joints as well as the absence of fatigue studies in the field of FSWed copper joints motivated the authors to investigate the subject. The current experimental study is conducted to exhibit the ambient LCF properties, and the mechanical behavior is discussed in light of cyclic hardening with changing strain amplitudes.

2. Experimental Procedure

2.1 Joint Fabrication and Microstructural Characterizations

Commercial purity copper plates with the nominal composition, shown in Table 1, and the dimensions of 150 mm × 100 mm × 4 mm were exposed to FSW with a tool rotational speed of 600 rpm and traverse speed of 45 mm/min utilizing a vertical CNC milling system. The schematic of the welding process used in the present study is demonstrated in Fig. 1. To reach a uniform structure with desirable hardening, copper plates were annealed in the furnace at 700 °C for 1 hour before FSW (Ref 23, 40). A high carbon steel cylindrical threaded tool was used with the shoulder diameter of 12 mm and the pin diameter and length of 5 and 3.6 mm, respectively. The FSW process was performed by controlling the plunge depth to be 0.3 mm with a tilt angle of 3°.

The samples for microstructural analysis were cut from the cross section of the joints perpendicular to the traverse direction. Specimens for optical microscopy (OM) were prepared by grinding, polishing, and etching by utilizing a mixture of distilled water, nitric acid, and acetic acid (7,2,1). OM and scanning electron microscopy (SEM) were employed to characterize the microstructural evolution and fracture surfaces, respectively.

2.2 Mechanical Characterization

Vickers microhardness tests with 1000 gf load were applied for determining the hardness on the cross-sectional area. Hardness profiles for the joint were prepared along the mid-thickness of the plate at an interval of 0.5 mm. Hardness measurements were used to quantify the cyclic behavior which can also be quantified by a non-dimensional parameter, $\frac{\Delta H}{H_i} =$

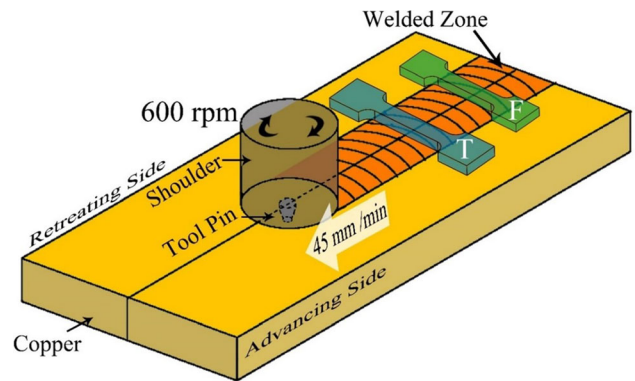


Fig. 1 Schematic of the FSW process including the geometry of tensile (*T*) and fatigue (*F*) samples

$\frac{(H_i - H_f)}{H_i}$ where H_i and H_f represent the hardness of the material before and after LCF testing (Ref 34).

Tensile tests were done at room temperature employing an Instron mechanical testing frame under a constant strain rate of 0.05 s⁻¹. Dog-bone-shaped tensile specimens with a gage length of 15 mm and width of 3 mm as well as fatigue samples with a gage length of 12 mm and width of 3 mm were electro-discharged machined from the welded plates, as illustrated in Fig. 1. The specimens were ground to achieve a smooth surface finish.

Following a similar method as those for the tensile tests, fatigue specimens were machined perpendicular to the welding direction. Total strain-controlled experiments were conducted with the strain ratio of $R = -1$ and at the frequency of 0.1 Hz. A sinusoidal waveform was employed at a strain amplitude range of 0.1 to 0.6%.

3. Results and Discussion

3.1 Microstructure and Monotonic Properties

The schematic of a cap-like welding zone after FSW is shown in Fig. 2(a). Four recognizable zones can be identified in the microstructure of FSWed pure copper (Fig. 2b-e), i.e., the NZ with severely deformed and nearly equiaxed grain structure, the thermo-mechanically affected zone (TMAZ) with elongated grains along the flow line, the heat affected zone (HAZ) with slightly larger grains and the BM (Ref 21, 41).

The microhardness profile throughout the cross section of the welded sample is illustrated in Fig. 3. The average microhardness of the BM was measured to be 102 HV after at least three tests from different zones with a standard deviation lower than 3%. The hardness of the weld zone is lower than the BM which is in agreement with previous results mentioning aluminum alloys and pure copper (Ref 41, 42). The competition between thermal exposure and grain refinement in

Table 1 Chemical composition of pure copper

B, %	Sb, %	Zn, %	Mn, %	Al, %	Fe, %	Ni, %	Al, %	Si, %	Cu, %
0.002	0.001	0.041	0.006	0.006	0.006	0.08	0.006	0.007	Balance

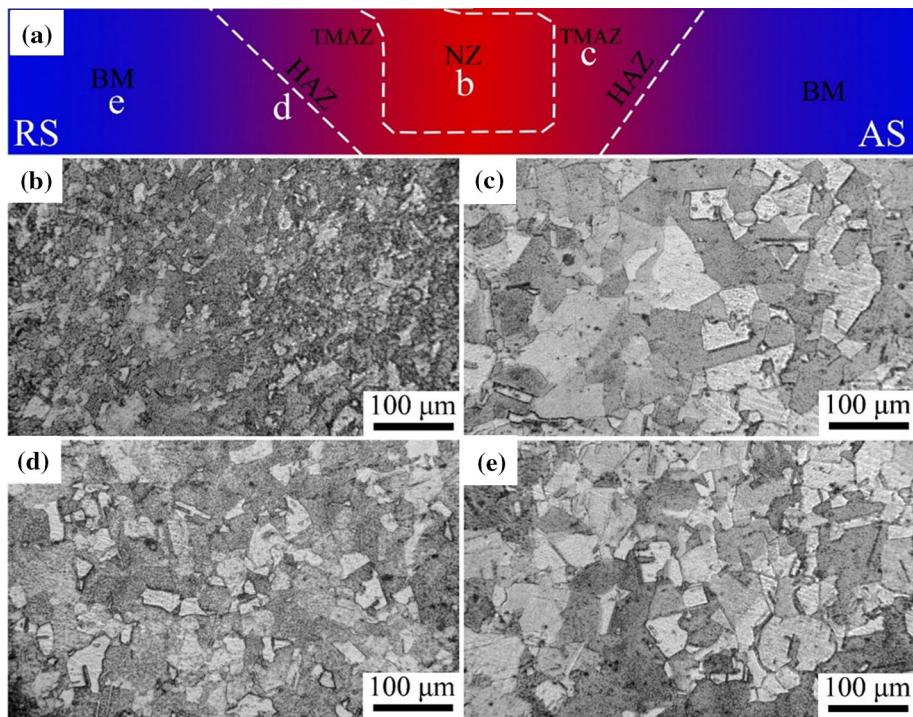


Fig. 2 (a) Cap-like welding zone in the pure copper microstructure demonstrating (b) the NZ (c) the TMAZ, (d) the HAZ, and (e) the BM

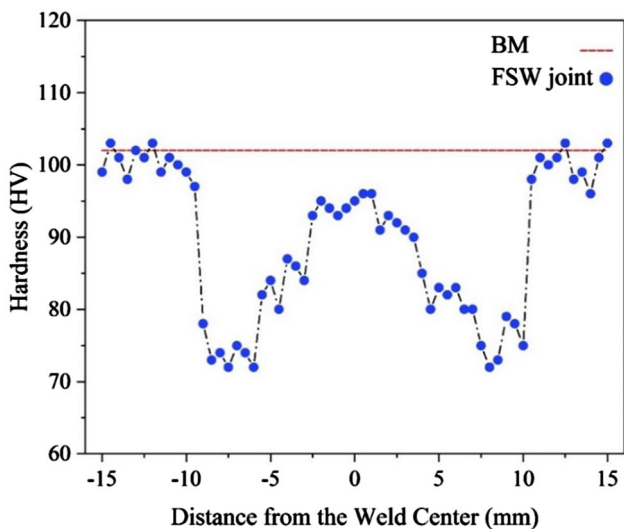


Fig. 3 Graph representing the average microhardness of the base metal along with the microhardness distribution across the weld line

NZ can affect the hardness of the joint. On the one hand, the occurrence of grain refinement is supposed to enhance the strength and hardness of NZ. On the other hand, high heat input during FSW deteriorates the hardness of the joint. In the present study, the softening stemmed from thermal exposure could not be completely compensated by the obtained level of grain refinement. Also, the lowest hardness is observed in the HAZ as related to the growth of a coarse-grained microstructure, exposed to excessive heat input.

Tensile properties of the BM and the FSW joint samples are illustrated in Table 2. The ultimate tensile strength values of joint samples are almost the same as the BM samples which can

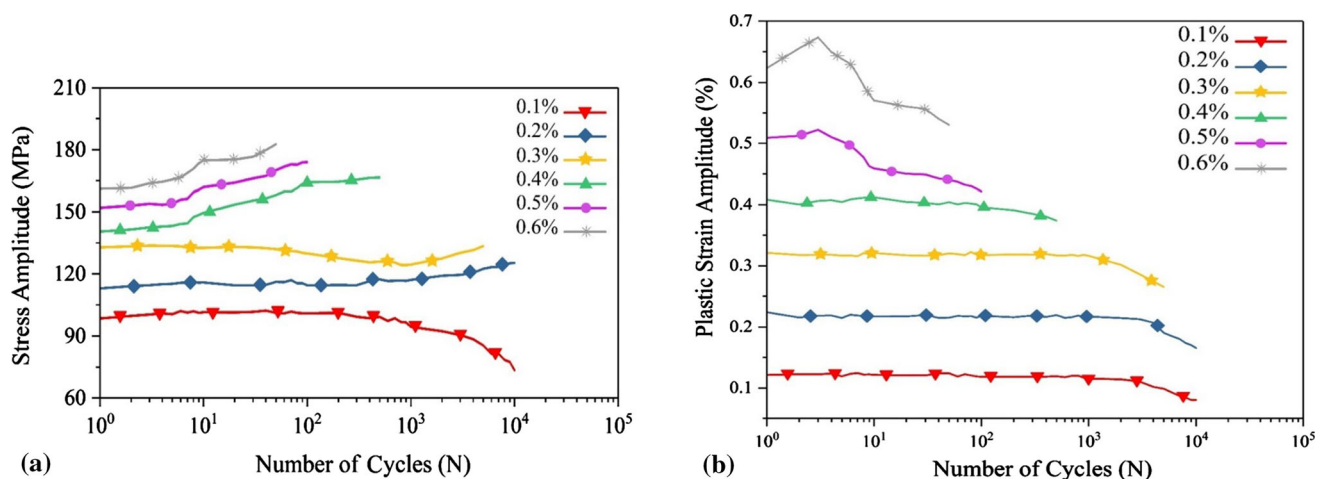
be attributed to the microstructural refinement during the process (Ref 43). Lower elongation of the joints can be attributed to the higher density of defects, e.g., dislocations, porosities and grain boundaries introduced during severe plastic deformation (Ref 44). These microstructural defects are sources for the initiation of cracks consequently causing a reduction in the ductility. Despite lower elongation, the joints show higher yield strength values in comparison with the BM. These observations can be supported by other works on FSWed copper (Ref 26, 43).

3.2 Cyclic deformation response

The stress and plastic strain amplitudes versus the number of cycles at different total strain amplitudes are demonstrated in Fig. 4a and b. It is obvious that by increasing the total strain amplitude, fatigue life decreases, while the stress amplitude increases. High strain amplitude promotes fatigue crack initiation and propagation causing an earlier fracture at relatively lower cycle numbers (Ref 45, 46). At the strain amplitude of 0.1%, the stress amplitude started to decrease significantly in cycles higher than 1000 indicating a cyclic softening. Cyclic softening was also reported at low strain amplitudes for severely deformed pure copper (Ref 34). It was mentioned that cyclic softening is due to the interactions between existent dislocations and introduced dislocations during cyclic loading. Softening was triggered principally by a reduction in the defect density in severely deformed copper and variations in boundary misorientation. It was also stated that cyclic softening in UFG copper can be due to the annihilation of dislocations with opposite signs and/or grain coarsening during cyclic loading (Ref 47, 48). Decrease in the dislocation density of subgrains or cell interiors can lead to distinct cyclic softening during LCF testing.

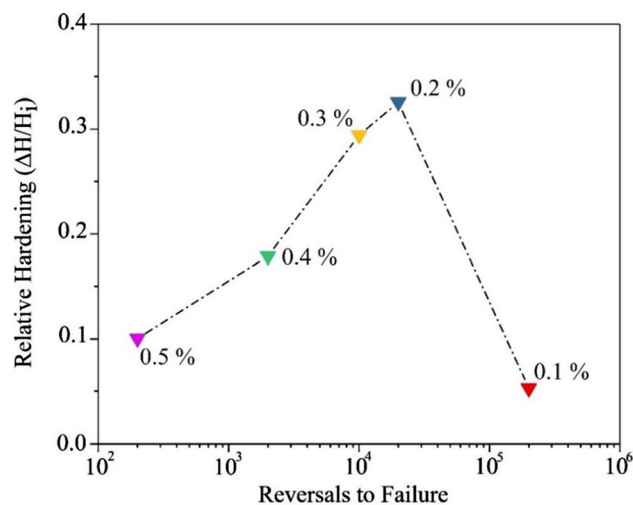
Table 2 Tensile properties of the base metal and FSW joint at a strain rate of 0.05 s^{-1}

Sample	YS, MPa	UTS, MPa	Elongation, %	E , GPa	n	K , MPa
Base Metal	86 ± 5	213 ± 8	48 ± 0.9	130 ± 2	0.42 ± 0.02	510 ± 3
FSW joint	104 ± 3	218 ± 3	46 ± 1.2	134 ± 3	0.41 ± 0.02	506 ± 3

**Fig. 4** (a) The stress and (b) plastic strain amplitudes versus the number of cycles at various total strain amplitudes for the FSW joint samples

At intermediate strain amplitudes of 0.2% and 0.3%, dominant hardening was observed following the stress plateau region. At an early stage, FSW joints showed a remarkable increase in the stress amplitude along with a gradual decrease in the plastic strain amplitude at high strain amplitudes of 0.5% and 0.6%. Comparing the current results with previous literature for pure copper, it is implied that the FSW process has a slight effect on the cyclic deformation behavior of pure copper joints (Ref 29, 34, 35). However, Huang et al. (Ref 35) observed the hardening effect at the total strain amplitudes of 0.1, 0.2, and 0.3% in the mid-life cycle for coarse-grained pure copper. Also, the hardening effect was observed for the strain amplitudes ranging from 0.2 to 0.6% in the current study. At a strain amplitude of 0.1%, a slight decrease in plastic strain amplitude is obvious after 1000 cycles. The same trend is evident for strain amplitudes of 0.2 and 0.3%. With the increase in strain amplitude to 0.4%, plastic strain amplitude begins to decrease at the early cycles of 10 and the same trend is recorded for the sample failure. A gradual decrease in plastic strain amplitude in relatively high strain amplitudes can be attributed to the decrease in the corresponding stress values, significantly influencing the strain values (Ref 23). Furthermore, as represented in Fig. 4, a ductile to brittle transition can be observed above the strain amplitude of 0.4%. Also, the respective damage mechanisms are addressed in Section 3.5. At the highest strain amplitude of 0.6%, an abrupt reduction in plastic strain amplitude is observed at early cycles which can be imputed to the sudden failure of the sample at the early stages of cycling (Ref 23).

Cyclic deformation response, quantified by a relative hardening/softening value of $\Delta H/H_i$, is exhibited according to the number of reversals to failure in Fig. 5. Starting from 200 cycles, a gradual increase in hardening can be observed up to about 20000 cycles. A higher number of cycles to failure leads

**Fig. 5** Relative hardening ($\Delta H/H_i$) versus reversals to failure for the FSW joint samples

to abrupt softening. The degree of softening for a high number of reversals to failure (low strain amplitude 0.1%) has a striking resemblance to the previous works on cold-rolled and annealed pure copper samples (Ref 34, 49). In these studies, the concept of never truly saturation (stress flowing) was described along with the occurrence of softening at the beginning of cyclic deformation due to low total strain amplitude (Ref 49, 50).

The cyclic behavior of pure copper at low strain amplitudes could be interpreted by the threshold stress corresponding to a certain strain amplitude below which the dislocation motion is not effective enough to re-organize the original substructure. (Ref 51). However, at high strain amplitudes the movement of dislocations is adequate to produce sustainable deformation and

hence could explain the relative hardening observed at a low number of reversals to failure (high total strain amplitude). The study of Vinogradov et al. (Ref 52) also claimed that severely deformed copper would present a lack of cyclic softening, but rather a relative hardening.

3.3 Hysteresis Behavior

The effect of cyclic loading on the mechanical properties of the joints was investigated using the hysteresis loops for the mid-life cycles of the BM and FSW joints at the constant strain amplitude of 0.2% are shown in Fig. 6. Hysteresis loops of the joints are comparatively larger, change in a wider range, and therefore present higher stress range for the FSW counterpart in the same strain amplitude. A relative concavity is seen for both samples (BM and FSW) in both ascending and descending phases. Small amount of linear loading and unloading portions were observed after the reversals followed by a major nonlinear response. The nonlinear features in the hysteresis loops have been attributed to the effect of deformation twinning in magnesium and aluminum alloys (Ref 39, 53). Although twinning is not common for coarse-grained pure copper, the severely deformed microstructure could be responsible for the activation of unexpected deformation modes (Ref 38). It is expected that the effect of inhomogeneous microstructure on the mechanical properties would accelerate the operation of new slip modes.

Figure 7 illustrates the hysteresis loops for the FSW joints at various total strain amplitudes, ranging from 0.1 to 0.6%. Starting from 0.1%, the cyclic response displays a hysteresis behavior. Approximately symmetrical and clockwise-rotation hysteresis loops are detected at high strain amplitudes of 0.3, 0.4, 0.5, and 0.6%. Similar hysteresis characteristics were formerly observed in ECAE processed pure copper (Ref 29). The area of a hysteresis loop indicates energy dissipation and loss per cycle (Ref 54). Accordingly, the area of hysteresis increases with a rise in strain amplitude, attesting considerable energy dissipation per cycle as connected to more severe dislocation activity, plastic deformation, and eventually causing crack nucleation (Ref 55).

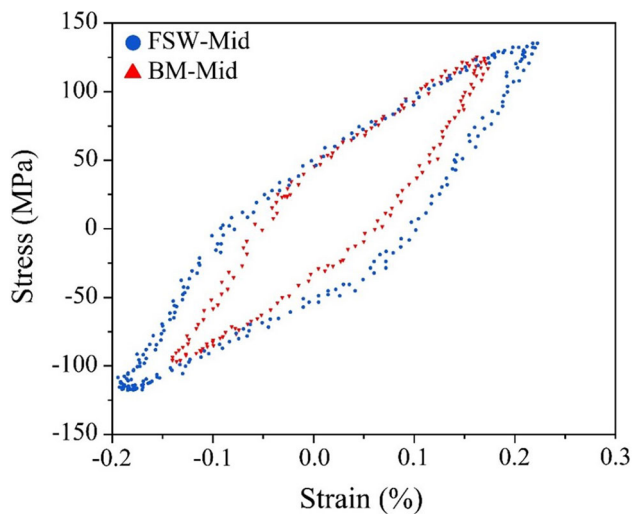


Fig. 6 Hysteresis behavior for the mid-life cycles of the BM and FSW joint samples at the constant strain amplitude of 0.2%

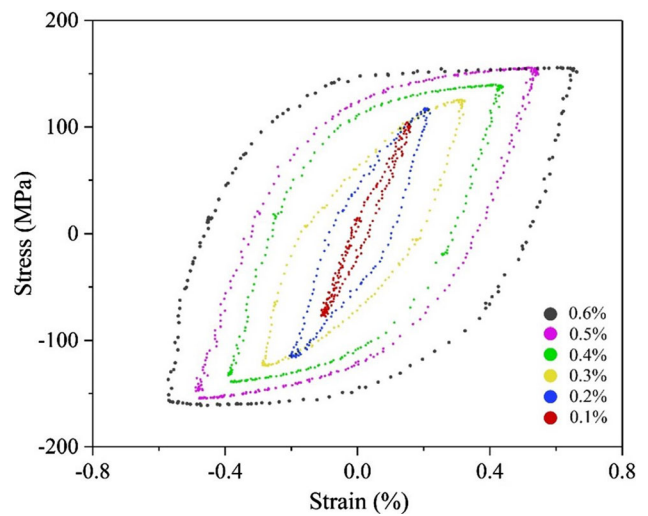


Fig. 7 Hysteresis behavior for the FSW joint samples at various strain amplitudes

Table 3 Strain-controlled fatigue parameters for the BM and FSW joint

LCF parameters	FSW joint	BM
Cyclic strain hardening exponent, n'	0.57	0.53
Coefficient of cyclic strength, K' , MPa	802	821
Coefficient of fatigue strength, σ'_f , MPa	645	573
Fatigue strength exponent, b	-0.32	-0.24
Fatigue ductility coefficient, ϵ'_f , %	0.1458	-0.18
Fatigue ductility exponent, c	-0.41	-0.45

3.4 Fatigue life and fatigue parameters

Using the Basquin and Coffin-Manson relationships (Ref 30, 53, 56), it can be inferred that the total strain amplitude consists of elastic and plastic amplitude regions which can be expressed by the following equations:

$$\frac{\Delta \epsilon_t}{2} = \frac{\Delta \epsilon_e}{2} + \frac{\Delta \epsilon_p}{2} = \frac{\sigma'_f (2N_f)^b}{E} + \epsilon'_f (2N_f)^c \quad (\text{Eq 1})$$

where E is the elastic modulus, N_f , σ'_f , and b are the number of cycles to failure, fatigue strength coefficient, and fatigue strength exponent, respectively. Also, ϵ'_f and c represent the fatigue ductility coefficient and the fatigue ductility exponent, respectively. The elastic strain amplitude is attributed to the Basquin's equation and the plastic strain component is interpreted by the Coffin-Manson relation, where the strain amplitude values are derived from the mid-life cycles.

Generally, it is assumed that only plastic strain would have a significant role in the softening/hardening behavior of fine-grained materials (Ref 30). Thus, the cyclic stress-strain response can be explained by the following equation (Ref 53, 56):

$$\frac{\Delta \sigma}{2} = K' \left(\frac{\Delta \epsilon_p}{2} \right)^{n'} \quad (\text{Eq 2})$$

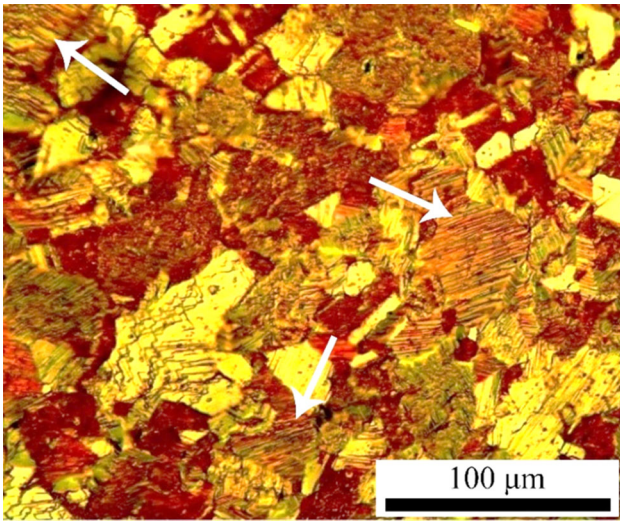


Fig. 8 Cellular substructure with embedded veins in the HAZ after fatigue loading at 0.1% strain amplitude

where K' is the cyclic strength coefficient, n' is the cyclic strain hardening exponent, $\Delta\sigma/2$ and $\Delta\epsilon_p/2$ are the stress amplitude and plastic strain amplitude of the mid-life cycles, respectively. The expected fatigue life parameters are summarized in Table 3, and the monotonic strain hardening exponent (n) can be compared with the cyclic hardening component (n') obtained at the same strain rate of 0.05 s^{-1} . Accordingly, the cyclic hardening exponent value is higher than the former, indicating significant hardening in loading with reversals as compared to that in monotonic straining. The cyclic strength coefficient K' is nearly the same for the FSW joint samples and the BM samples while the values for fatigue strength and ductility coefficients (σ'_f and ϵ'_f) are higher for the former indicating higher cyclic strength and ductility. It should also be noted that these findings are representative of the joint samples fabricated by the specific processing parameter set used herein.

3.5 Fracture Behavior

Fracture surfaces of the fatigued samples were analyzed using OM and SEM. The FSW joints were mostly inclined to fracture in the HAZ rather than the NZ. The failure location is related to grain coarsening and microstructural instabilities in the HAZ (Ref 29, 57). Fine and homogeneous grains in the NZ have led to high tensile strength and improved fatigue behavior transferring the fracture location to a more vulnerable, unstable region in the HAZ. Fig. 8 shows the resulting microstructure of HAZ after testing at the low strain amplitude of 0.1%. The HAZ microstructure has relatively equiaxed grains with observable misorientations between them. It is suggested that the formation of secondary slip bands, indicated by white arrows, could activate new slip systems (Ref 35). It is also reported that at low strain amplitudes, insufficient plastic strain may result in the formation of a cellular substructure with embedded veins (Ref 35, 58).

Fracture surfaces of the FSW joints were also studied after fatigue loading to help recognize the failure mechanisms by identifying cracked zones along with the regions of crack initiation and propagation. Fig. 9 shows the fracture surfaces for sample fatigued at strain amplitudes of 0.5% and 0.1%. The fracture surface was generally flat, and no inclined zone was

observed in the fracture area after fatigue at the strain amplitude of 0.5% (Fig. 9a-c). Crack initiation and propagation were observed from multiple origins and along various routes, respectively, as pointed on the fracture surface of the sample strained at the amplitude of 0.5% (Fig. 9a and b). It is proposed that final separation occurs when multiple cracks merge along the weakest path (Ref 53). As the cracks mostly initiated from the surface of the samples, this observation can be imputed to the cyclic slip irreversibility (Ref 59). During cyclic deformation, few dislocations may arrive at the free surface of the sample, but they do not return back to the sample for reverse loading. This causes the formation of defects near the surface of the component and eventually leads to the initiation of fatigue cracks. For the aforementioned sample, relatively large cracks were found within the fracture zone (Fig. 9b and c).

Crack initiation zones are also apparent in the sample strained at the low strain amplitude of 0.1% (Fig. 9e). On the other hand, more dimples are observed in this sample (Fig. 9f) indicating a relatively more ductile fracture behavior. It is stated that at low strain amplitudes, a step is formed during fracture by the collision of two fatigue cracks. This characterizes the overload detachment by the clash of the two cracks propagated at different planes (Ref 60). Total fatigue life can be calculated from the total number of cycles for crack initiation and propagation. With rise in the strain amplitude, both crack initiation and propagation lives would be degraded causing a sharp decrease in the total fatigue life. It is also worth noting that in the LCF regime, crack propagation dominates the total fatigue life; as such resistance to fatigue crack growth is known to be inferior in UFG materials containing high density of defects (Ref 61, 62).

4. Conclusions

Cyclic deformation characteristics, fatigue life, fatigue parameters, and fracture behavior of pure copper joints fabricated by FSW were investigated in the strain-controlled regime along with monotonic loading response and hardness properties. The following conclusions can be drawn:

1. Defect-free joints of pure copper were achieved using FSW producing a nugget zone with nearly equiaxed microstructure as a result of the severe plastic deformation. The FSW joints showed relatively high yield strength with about 20% improvement over the BM and uniform elongation exceeding 25%.
2. For the employed set of FSW parameters, at the low strain amplitude of 0.1%, softening occurred while cyclic hardening was detected at higher strain amplitudes. By increasing the total strain amplitude, the plastic strain amplitude begins to decrease at high number of cycles, and the stress amplitude increases.
3. The cyclic hardening exponent value (n') is higher for the FSW joint relative to the BM, indicating significant hardening in loading with reversals as compared to that in monotonic straining. The values for fatigue strength and ductility coefficients (σ'_f and ϵ'_f) are higher for the joint samples manufactured by the utilized FSW parameters indicating higher cyclic strength and ductility for the FSW joint.

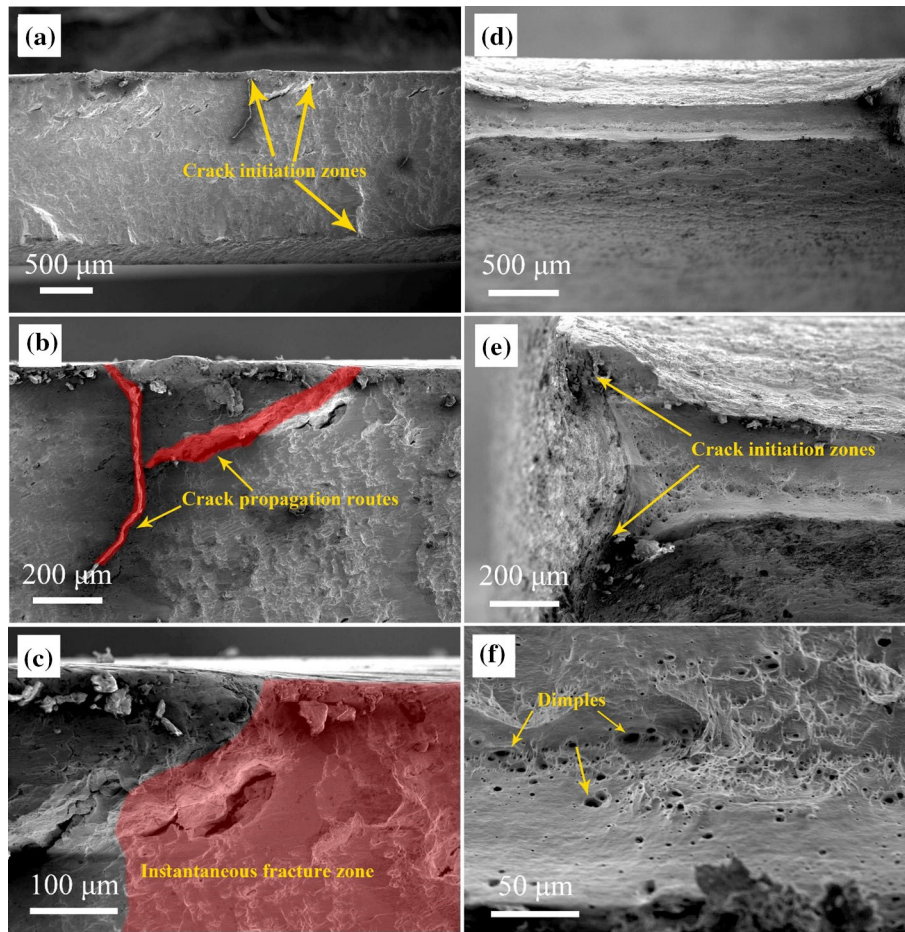


Fig. 9 Fracture surfaces of FSW joints after fatigue loading, (a-c) at the strain amplitude of 0.5%, and (d-f) at the strain amplitude of 0.1% with different magnifications

4. The FSW joints mostly fractured in the HAZ rather than the NZ, featuring higher cyclic strength of the FSW joints. Microstructural evolution following cyclic deformation revealed the formation of secondary slip bands.
5. Fracture morphology examinations illustrated a ductile behavior represented by fracture surfaces covered by dimples for the samples tested at 0.1% cyclic strain amplitude; while the samples strained at 0.5% showed a brittle fracture with cracks originating from multiple sites, pointing to the manifestation of a ductile to brittle transition with varying plastic strain.

Acknowledgments

Support from Ozyegin University Research Fund is acknowledged.

References

1. J.-W. Lin, H.-C. Chang, and M.-H. Wu, Comparison of Mechanical Properties of Pure Copper Welded Using Friction Stir Welding and Tungsten Inert Gas Welding, *J. Manuf. Process.*, 2014, **16**(2), p 296–304
2. H. Khodaverdizadeh, A. Heidarzadeh, and T. Saeid, Effect of Tool Pin Profile on Microstructure and Mechanical Properties of Friction Stir Welded Pure Copper Joints, *Mater. Des.*, 2013, **45**, p 265–270
3. W. Oates, *Welding Handbook-Materials and Applications-Part 1*, Vol 3 AWS, Miami, 1996
4. S.A.A. Akbari Mousavi and S.T. Niknejad, An Investigation on Microstructure and Mechanical Properties of Nd:YAG Laser Beam Weld of Copper Beryllium Alloy, *Metall. Mater. Trans. A*, 2009, **40**(6), p 1469–1478
5. B. Venu, I. BhavyaSwathi, L.S. Raju, G. Santhanam, A Review on Friction Stir Welding of Various Metals and Its Variables, *Mater. Today: Proc.*, 2019, **18**, p 298–302
6. X. Meng, Y. Huang, J. Cao, J. Shen, and J.F. dos Santos, Recent Progress on Control Strategies for Inherent Issues in Friction Stir Welding, *Prog. Mater. Sci.*, 2021, **115**, p 100706
7. I.J. Ibrahim and G.G. Yapici, Application of a Novel Friction Stir Spot Welding Process on Dissimilar Aluminum Joints, *J. Manuf. Process.*, 2018, **35**, p 282–288
8. R.S. Mishra and Z.Y. Ma, Friction Stir Welding and Processing, *Mater. Sci. Eng. R. Rep.*, 2005, **50**(1–2), p 1–78
9. A. Rashidi, A. Mostafapour, V. Rezazadeh, and S. Salahi, Channel Formation in Modified Friction Stir Channeling, *Appl. Mech. Mater.*, 2013, **302**, p 371–376
10. A. Rashidi, A. Mostafapour, V. Rezazadeh, and S. Salahi, Modified Friction Stir Channeling: A Novel Technique for Fabrication of Friction Stir Channel, *Appl. Mech. Mater.*, 2013, **302**, p 365–370
11. A. Heidarzadeh, A. Radi, and G.G. Yapici, Formation of Nano-Sized Compounds During Friction Stir Welding of Cu-Zn Alloys: Effect of Tool Composition, *J. Market. Res.*, 2020, **9**(6), p 15874–15879

12. K. Chen, W. Gan, K. Okamoto, K. Chung, and R. Wagoner, The Mechanism of Grain Coarsening in Friction-Stir-Welded AA5083 after Heat Treatment, *Metall. Mater. Trans. A.*, 2011, **42**(2), p 488–507
13. E. Cerri and P. Leo, Warm and Room Temperature Deformation of Friction Stir Welded Thin Aluminium Sheets, *Mater. Des.*, 2010, **31**(3), p 1392–1402
14. X. Cao and M. Jahazi, Effect of Welding Speed on the Quality of Friction Stir Welded Butt Joints of A Magnesium Alloy, *Mater. Des.*, 2009, **30**(6), p 2033–2042
15. K. Nakata, Friction Stir Welding of Copper and Copper Alloys, *Weld. Int.*, 2005, **19**(12), p 929–933
16. R. Abrahams, J. Mikhail, and P. Fasihi, Effect of Friction Stir Process Parameters on the Mechanical Properties of 5005-H34 and 7075-T651 Aluminium Alloys, *Mater. Sci. Eng. A*, 2019, **751**, p 363–373
17. A.H. Baghdadi, A. Rajabi, N.F.M. Selamat, Z. Sajuri, and M.Z. Omar, Effect of Post-Weld Heat Treatment on the Mechanical Behavior and Dislocation Density of Friction Stir Welded Al6061, *Mater. Sci. Eng. A*, 2019, **754**, p 728–734
18. A. Hosseinzadeh and G.G. Yapici, High Temperature Characteristics of Al2024/SiC Metal Matrix Composite Fabricated by Friction Stir Processing, *Mater. Sci. Eng. A*, 2018, **731**, p 487–494
19. T. Sakthivel, and J. Mukhopadhyay, Microstructure and Mechanical Properties of Friction Stir Welded Copper, *J. Mater. Sci.*, 2007, **42**(19), p 8126–8129
20. A. Abdollah-Zadeh, T. Saeid, and B. Sazgari, Microstructural and Mechanical Properties of Friction Stir Welded Aluminium/Copper Lap Joints, *J. Alloy. Compd.*, 2008, **460**(1–2), p 535–538
21. R. Nandan, T. DebRoy, and H. Bhadeshia, Recent advances in Friction-Stir Welding—Process, Weldment Structure and Properties, *Prog. Mater. Sci.*, 2008, **53**(6), p 980–1023
22. R. Rzaev, A. Chularis, V. Smirnov, and L. Semyenova, The Influence of the Friction Stir Welding Parameters on the Formation of Welded Joint of Aluminum and Copper Alloys, *Mater. Today Proc.*, 2019, **11**, p 534–542
23. S. Salahi, V. Rezaeadeh, A. Iranizad, A. Hosseinzadeh, and A. Safari, *Microstructure and Mechanical Properties of Friction Stir Welded Annealed Pure Copper Joints*, *Advanced Materials Research*, Trans Tech Publ, Stafa, 2013, p 346–351
24. G.M. Xie, Z.Y. Ma, and L. Geng, Development of a Fine-Grained Microstructure and the Properties of a Nugget Zone in Friction Stir Welded Pure Copper, *Scr Mater.*, 2007, **57**(2), p 73–76
25. H.J. Liu, J.J. Shen, Y.X. Huang, L.Y. Kuang, C. Liu, and C. Li, Effect of Tool Rotation Rate on Microstructure and Mechanical Properties of Friction Stir Welded Copper, *Sci. Technol. Weld. Join.*, 2009, **14**(6), p 577–583
26. A. Heidarzadeh, T. Saeid, H. Khodaverdizadeh, A. Mahmoudi, and E. Nazari, Establishing a Mathematical Model to Predict the Tensile Strength of Friction Stir Welded Pure Copper Joints, *Metall. Mater. Trans. B*, 2013, **44**(1), p 175–183
27. D. Ni, D. Chen, B. Xiao, D. Wang, and Z. Ma, Residual Stresses and High Cycle Fatigue Properties of Friction Stir Welded SiCp/AA2009 Composites, *Int. J. Fatigue*, 2013, **55**, p 64–73
28. D. Hrishikesh, D. Chakraborty, and T.K. Pal, High-Cycle Fatigue Behavior of Friction Stir Butt Welded 6061 Aluminium Alloy, *Trans. Nonferrous Met. Soc. China*, 2014, **24**(3), p 648–656
29. H. Maier, P. Gabor, and I. Karaman, Cyclic Stress–Strain Response and low-Cycle Fatigue Damage in Ultrafine Grained Copper, *Mater. Sci. Eng. A*, 2005, **410**, p 457–461
30. D. Ni, D. Chen, J. Yang, and Z. Ma, Low Cycle Fatigue Properties of Friction Stir Welded Joints of a Semi-Solid Processed AZ91D Magnesium Alloy, *Mater. Des.*, 2014, **56**, p 1–8
31. Z. Zhang, Z. Wang, and Z. Sun, Evolution and Microstructural Characteristics of Deformation Bands in Fatigued Copper Single Crystals, *Acta Mater.*, 2001, **49**(15), p 2875–2886
32. P. Li, S. Li, Z. Wang, and Z. Zhang, Formation Mechanisms of Cyclic Saturation Dislocation Patterns in [001], [011] and Copper Single Crystals, *Acta Mater.*, 2010, **58**(9), p 3281–3294
33. S. Qu, X. An, H. Yang, C. Huang, G. Yang, Q. Zang, Z. Wang, S. Wu, and Z. Zhang, Microstructural Evolution and Mechanical Properties Of Cu-Al Alloys Subjected to Equal Channel Angular Pressing, *Acta Mater.*, 2009, **57**(5), p 1586–1601
34. S. Agnew and J. Weertman, Cyclic Softening of Ultrafine Grain Copper, *Mater. Sci. Eng. A*, 1998, **244**(2), p 145–153
35. H. Huang, S. Mao, D. Gan, and N. Ho, The Strain Amplitude Controlled Fatigue Behavior of Pure Copper with Ultra Large Grain Size, *Mater. Sci. Eng. A*, 2013, **559**, p 170–177
36. D. Kuhlmann-Wilsdorf and C. Laird, Dislocation Behavior in Fatigue V: Breakdown of Loop Patches and Formation of Persistent Slip Bands and of Dislocation Cells, *Mater. Sci. Eng.*, 1980, **46**(2), p 209–219
37. C. Laird, P. Charsley, and H. Mughrabi, Low Energy Dislocation Structures Produced by Cyclic Deformation, *Mater. Sci. Eng.*, 1986, **81**, p 433–450
38. C. Liu, M. Bassim, and D. You, Dislocation Structures in Fatigued Polycrystalline Copper, *Acta Metall. Mater.*, 1994, **42**(11), p 3695–3704
39. M. Czechowski, Low-Cycle Fatigue of Friction Stir Welded Al-Mg Alloys, *J. Mater. Process. Technol.*, 2005, **164**, p 1001–1006
40. S. Salahi and V. Rezaeadeh, Fracture Mechanism in Friction Stir Processed Annealed Pure Copper Samples, *World Appl. Sci. J.*, 2013, **23**(12), p 54–58
41. H. Khodaverdizadeh, A. Mahmoudi, A. Heidarzadeh, and E. Nazari, Effect of Friction Stir Welding (FSW) Parameters on Strain Hardening Behavior of Pure Copper Joints, *Mater. Des.*, 2012, **35**, p 330–334
42. K. Elangovan and V. Balasubramanian, Influences of pin Profile and Rotational Speed of the Tool on the Formation of Friction Stir Processing Zone in AA2219 Aluminium Alloy, *Mater. Sci. Eng. A*, 2007, **459**(1), p 7–18
43. W.-B. Lee and S.-B. Jung, The Joint Properties of Copper by Friction Stir Welding, *Mater. Lett.*, 2004, **58**(6), p 1041–1046
44. A. Heidarzadeh and T. Saeid, A Comparative Study of Microstructure and Mechanical Properties Between Friction Stir Welded Single and Double Phase Brass Alloys, *Mater. Sci. Eng. A*, 2016, **649**, p 349–358
45. S. Begum, D.L. Chen, S. Xu, and A.A. Luo, Low Cycle Fatigue Properties of an Extruded AZ31 Magnesium Alloy, *Int. J. Fatigue*, 2009, **31**(4), p 726–735
46. I. Nikulin, T. Sawaguchi, A. Kushibe, Y. Inoue, H. Otsuka, and K. Tsuzaki, Effect of Strain Amplitude on the Low-Cycle Fatigue Behavior of a New Fe-15Mn-10Cr-8Ni-4Si Seismic Damping Alloy, *Int. J. Fatigue*, 2016, **88**, p 132–141
47. H.W. Höppel, Z.M. Zhou, H. Mughrabi, and R.Z. Valiev, Microstructural Study of the Parameters Governing Coarsening and Cyclic Softening in Fatigued Ultrafine-Grained Copper, *Philos. Mag. A*, 2002, **82**(9), p 1781–1794
48. M.W. Kapp, T. Kremmer, C. Motz, B. Yang, and R. Pippan, Structural Instabilities During Cyclic Loading of Ultrafine-Grained Copper Studied with Micro Bending Experiments, *Acta Mater.*, 2017, **125**, p 351–358
49. C. Feltner and C. Laird, Cyclic Stress-Strain Response of FCC Metals and Alloys: I Phenomenological Experiments, *Acta Metall.*, 1967, **15**(10), p 1621–1632
50. P. Sanders, J. Eastman, and J. Weertman, Elastic and Tensile Behavior of Nanocrystalline Copper and Palladium, *Acta Mater.*, 1997, **45**(10), p 4019–4025
51. C. Laird, Z. Wang, B.-T. Ma, and H.-F. Chai, Low energy Dislocation Structures Produced by Cyclic Softening, *Mater. Sci. Eng. A*, 1989, **113**, p 245–257
52. A. Vinogradov, Y. Kaneko, K. Kitagawa, S. Hashimoto, V. Stoliarov, and R. Valiev, Cyclic Response of Ultrafine-Grained Copper at Constant Plastic Strain Amplitude, *Scripta Mater.*, 1997, **36**(11), p 1345–1351
53. H. Patel, D. Chen, S. Bhole, and K. Sadayappan, Cyclic Deformation and Twinning in a Semi-Solid Processed AZ91D Magnesium Alloy, *Mater. Sci. Eng. A*, 2010, **528**(1), p 208–219
54. S.V. Sajadifar, G.G. Yapici, E. Demler, P. Krooß, T. Wegener, H. Maier, and T. Niendorf, Cyclic Deformation Response of Ultra-Fine Grained Titanium at Elevated Temperatures, *Int. J. Fatigue*, 2019, **122**, p 228–239
55. H.-G. Lambers, C. Rüsing, T. Niendorf, D. Geissler, J. Freudenberg, and H. Maier, On the Low-Cycle Fatigue Response of Pre-Strained Austenitic Fe61Mn24Ni6.5Cr8.5 Alloy Showing TWIP Effect, *Int. J. Fatigue*, 2012, **40**, p 51–60
56. S. Begum, D. Chen, S. Xu, and A.A. Luo, Strain-controlled Low-Cycle Fatigue Properties of a Newly Developed Extruded Magnesium Alloy, *Metall. Mater. Trans. A*, 2008, **39**(12), p 3014–3026
57. A. Alavi Nia and A. Shirazi, An Investigation into the Effect of Welding Parameters on Fatigue Crack Growth Rate and Fracture

- Toughness in Friction Stir Welded Copper Sheets, *Proc. Inst. Mech. Eng. Part L J. Mater. Des. Appl.*, 2018, **232**(3), p 191–203
58. S.-W. Mao, C.-W. Chang, H.-L. Huang, and N.-J. Ho, Evolution of Dislocations in Large Grains of Polycrystalline Copper Under Low Cycle Fatigue with Reduced Strain Amplitude, *Mater. Sci. Eng. A*, 2010, **527**(24), p 6489–6493
 59. H. Mughrabi, Cyclic Slip Irreversibilities and the Evolution of Fatigue Damage, *Metall. Mater. Trans. B.*, 2009, **40**(4), p 431–453
 60. O.F. Higuera-Cobos, J.A. Berríos-Ortiz, and J.M. Cabrera, Texture and Fatigue Behavior of Ultrafine Grained Copper Produced by ECAP, *Mater. Sci. Eng. A*, 2014, **609**, p 273–282
 61. S.V. Sajadifar, T. Wegener, G. Yapici, and T. Niendorf, Effect of Grain Size on the Very High Cycle Fatigue Behavior and Notch Sensitivity of Titanium, *Theor. Appl. Fract. Mech.*, 2019, **104**, p 102362
 62. A. Vinogradov, Fatigue Limit, and Crack Growth in Ultra-Fine Grain Metals Produced by Severe Plastic Deformation, *J. Mater. Sci.*, 2007, **42**(5), p 1797–1808

Publisher's Note Springer Nature remains neutral with regard to jurisdictional claims in published maps and institutional affiliations.